

Imprints of $U_A(1)$ chiral anomaly and disorder in the Dirac eigenspectrum of QCD at finite temperature

Ravi Shanker,^{1,*} Harshit Pandey,¹ and Sayantan Sharma¹

¹*The Institute of Mathematical Sciences, a CI of Homi Bhabha National Institute, Chennai 600113, India*

We perform a comprehensive study of the properties of Dirac eigenvalue spectrum in QCD as a function of temperature on the lattice. In addition to effects due to interplay between interactions and disorder inherently present in a many-body system, the Dirac spectrum also contains crucial information about the effective restoration of different subgroups of almost exact two flavor chiral symmetry in QCD. We calculate the infrared eigenvalues of the overlap Dirac operator on 2+1 flavor QCD ensembles generated using domain wall fermion discretization, on a large volume lattice. From the normalized level spacing ratios we identify those eigenvalues which have *intermediate* level statistics, distinctly different from the majority in the bulk spectrum that follow universal level fluctuations similar to a random matrix of Gaussian unitary type. We provide an explanation of these *intermediate* level ratios in terms of a specific random matrix model and quantify correlation between these eigenstates and disorder in the gauge fields manifested in the renormalized Polyakov loop values. Whereas existence of these *intermediate* eigenmodes are intimately connected to the effective restoration of different subgroups of chiral symmetry close to chiral crossover transition, these arise due to effects of random uncorrelated disorder at higher temperatures when the $U_A(1)$ is *effectively restored*. We also, for the first time, calculate the Thouless conductance for the Dirac spectrum that quantifies the structural rigidity of the eigenvectors, and use it as a diagnostic tool to understand the restoration of the anomalous $U_A(1)$ subgroup of chiral symmetry and localization driven due to disorder.

PACS numbers: 12.38.Gc, 11.15.Ha, 11.30.Rd, 11.15.Kc

I. INTRODUCTION

Interacting many-body quantum systems continue to challenge our understanding of fundamental processes like thermalization and transport. Understanding the universal properties of the eigenvalue spectra of the Hamiltonians describing such systems provides valuable insights about their dynamics. The universal fluctuations of the level spacings between adjacent energy eigenvalues is one such observable. Bohigas-Giannoni-Schmit conjecture [1] states that for quantum systems whose classical dynamics is non-integrable, the universal fluctuations of the level separations between eigenvalues of the Hamiltonian belong to one of the three universality classes of Wigner-Dyson statistics within Random Matrix theory (RMT). On the other hand if the corresponding classical dynamics is completely integrable, then the quantum energy eigenvalues behave like a sequence of independent random variables according to Berry-Tabor conjecture [2]. Therefore studying the universal level spacing fluctuations of a quantum system allows us to learn about the classical dynamics and vice versa, in particular, it allows us to understand how classical (non-)integrability manifests itself in the quantum many-body theory. This is important since it is expected that in classical non-integrable many body systems, the long-time dynamics characterized by ergodicity and mixing in the phase space, is universally governed by a thermal fixed point.

However the connection between chaos and thermalization is not very apparent in a quantum system [3].

Many realistic physical systems far from integrability exhibit quasi-periodic motion which is challenging to understand even from a purely classical point of view, let alone understanding the classical-quantum correspondence in these systems [4]. Some ideas inspired from semiclassical correspondence have been put forward by Berry and Robnik, who proposed that the spectral statistics of such mixed systems should be understood as arising from an uncorrelated superposition of spectra from different universality classes, each spectrum being associated with a chaotic or regular regions in classical phase space [5]. However extensive investigations [4, 6, 7] reveal that the universal fluctuations of the energy spectrum characterized in terms of integrable (ordered) as well as non-integrable (disordered) regions might be correlated, even in cases where no classical analog might exist [8–13] or the ordered (integrable) spectra may become chaotic due to strong admixture. There can be other non-trivial scenarios as well. Many-body systems can undergo localization transitions when symmetries of the Hamiltonian are broken as a function of external parameters, for e.g., the strength of disorder leading to a change in the nature of level fluctuations. Such cases are typically addressed by random matrix ensembles which interpolates between Poissonian and Wigner-Dyson level statistics as observed in localization transitions for e.g., close to the mobility edge [14] in the Anderson model [15]. In this particular case the critical eigenstates for very closely spaced eigenvalues are strongly correlated and have significant overlap with each other in spite of their sparse fractal-like

* Corresponding author: rshanker@imsc.res.in

structure. However very small correlations exist between eigenvalues with large separations.

An example of a strongly interacting many body quantum system, which has all these features is described by a non-Abelian gauge theory known as Quantum Chromodynamics (QCD). The QCD Hamiltonian is difficult to realize in three dimensions, instead we study the spectral properties of the QCD Dirac operator in Euclidean 3+1 dimensions. The Dirac eigenspectrum consisting of both localized as well as disordered eigenstates not only determines the localization and thus transport properties in QCD [16] but also explains key features of a non-trivial thermodynamic chiral (phase) transition [17, 18]. Thus, a strongly interacting many body system described by QCD is an important example of a theorist's laboratory to study how in addition to the interplay between disorder and interactions, the correlations due to the criticality related to the chiral phase transition gets imprinted in the level spacing statistics of the Dirac eigenvalues. This work is a detailed study on the QCD Dirac spectrum which provides new insights and ways to disentangle the features due to change in the localization (transport) properties as a function of temperature from those due to spontaneous breaking of different subgroups of chiral symmetry.

II. BACKGROUND

The eigenvalue spectrum of the Dirac operator provides important insights regarding the symmetries of QCD and their breaking. One particular eigenstate of the Dirac operator describes a one-particle massless fermion (quark) state in presence of a gauge background. The gauge fields provide both the interactions and the disorder whose strength changes with the temperature. The properties of the eigenvalue spectrum of the QCD Dirac operator, in presence of gauge ensembles have been studied extensively using lattice QCD at zero as well as finite temperatures. The intercept of the near-zero eigenmodes of the Dirac operator in the chiral symmetry broken phase gives an accurate estimate of the chiral condensate, the order parameter of the chiral phase transition in the limit of massless quarks. At temperatures $T < T_{pc}$, where $T_{pc} \sim 156.5$ MeV is the pseudo-critical temperature [19–21] corresponding to the chiral crossover transition in QCD with physical quark flavors, the level statistics of the deep infrared part of the spectrum can be explained within the universality class of RMT consisting of chiral Gaussian unitary ensemble (GUE) [22–25] whereas for the higher eigenvalues the universal features can be explained within Wigner's classification with a RMT ensemble of conventional GUE.

At higher temperatures, when the non-singlet part of the almost exact two-flavor chiral symmetry is *effectively* restored the intercept vanishes leading to the formation of a small peak-like feature in the infrared part of the eigenvalue spectrum. This peak has been observed in studies

using a mixed-action set-up [26–28] which was debated for a while [29–32]. However the existence of the peak was shown using dynamical domain wall fermions [33] on a finite lattice, now also observed to survive in the continuum limit in 2+1 QCD with HISQ discretization [34]. The higher (bulk) eigenvalues λ are disordered, whose density shows a linear in λ rise and their level spacing ratios are consistent with the predictions from RMT belonging to the GUE. The peak-like feature and the linearly rising bulk spectra overlap strongly, resulting in eigenvectors which are delocalized [35–37] but not ergodic and whose level spacing fluctuations are *intermediate* between the Poissonian and GUE values [38]. These infrared eigenvalues are characteristic of a strongly-coupled regime [35, 39, 40] and exhibit fractal-like features [38]. The median of the distribution of the fractal dimension D_f for these *intermediate* eigenvalues are tantalizingly similar to the expectations from an $O(4)$ spin model [38]. In contrast, the bulk eigenfunctions are delocalized and hence ergodic. The $U_A(1)$ subgroup will be *effectively* restored at a temperature, $T_{U(1)}$, when physical observables which are sensitive to it, e.g., the topological susceptibility has a temperature dependence that is consistent with that expected from a dilute gas of instantons. This can be motivated from the fact that once an onset to the dilute instanton regime occurs, there are no further changes in the topological properties even when the temperature is increased to asymptotically large values. The $T_{U(1)}$ is expected to be $\gtrsim 1.5 T_{pc}$ inferred from the temperature dependence of the topological susceptibility in QCD [41], from the features in the Dirac eigenvalue spectrum [26, 37], from the degeneracy of temporal meson correlators [42] and through tensor singlet channels [43]. A weaker bound $T_{U(1)} \gtrsim 1.2 T_{pc}$ was obtained from the eigenvalue spectrum of the HISQ Dirac operator in the continuum limit [34].

The scenario at even higher temperatures $T > T_{U(1)}$ is not yet well understood. Whereas a $m^2\delta(\lambda)$ peak-like feature of zero modes should survive expected from a dilute gas-like scenario of instantons [26, 37, 44, 45] it is heavily suppressed as a function of temperature contributing to the topological susceptibility which decreases as $\sim T^{-8}$ [41, 46, 47]. Eventually these infrared modes should be gapped out from the bulk part of the eigenvalue spectrum. Recent studies indicate that at sufficiently high temperatures, the most infrared part of this bulk spectrum contains localized eigenvalues which can be distinguished from the other delocalized bulk eigenmodes, which follow GUE level statistics, through a mobility edge [28, 48, 49]. This phenomenon is analogous to a localization transition [28, 49–54] observed in the Anderson model [15]. Nonetheless, a naive Anderson-like scaling of its temperature dependence demonstrates that the mobility edge might vanish at the pseudo-critical temperature [28, 50, 55], but it might also disappear only at the critical temperature which is achieved in the chiral limit [49]. The robustness of these observations will in future be tested through carefully performed infinite

volume and continuum extrapolations.

To summarize, whereas there is a wealth of results on spectral signatures related to *effective* restoration of the different subgroups of chiral symmetry, and on the localization properties through an Anderson-like transition, separately, the interplay between these two physically distinct phenomena is not so clear. We want to emphasize here that these two phenomena are of distinct physical origin and thus their consequences will also be different. Anderson transition is a quantum phase transition which, strictly speaking, is a zero temperature phenomenon. A possible way to understand such a (de-)localization transition at finite temperature is to relate the change in disorder as a function of temperatures; however a clear connection between the two is not very apparent. In QCD varying the temperature also results in the sequential (effective) restoration of different subgroups of chiral symmetry. Evidences suggest that the restoration of the $SU_A(2)$ occurs through a second order phase transition in the chiral limit, remnant effects of which will remain in the Dirac eigenvalue spectrum even for physical light quarks [38]. The effective restoration of $U_A(1)$ will result in characteristic changes in the localization properties of the Dirac eigenvectors, on the other hand an Anderson-like transition also results in structural changes in the eigenvectors of Dirac operator. It is thus imperative to disentangle these two phenomena, to unambiguously identify the mechanism that is causing such effects. However the temperature regime where these occur seems to overlap which makes it challenging to unambiguously separate these effects.

III. AN OUTLINE OF THIS WORK

In this work we provide a new way of disentangling the impact of *effective* restoration of $U_A(1)$ and the onset of localization of the 1-particle quark states in terms of the Dirac eigenspectrum. We show here that both these distinct physical phenomena are known to affect the infrared part of eigenspectrum of the QCD Dirac operator, at temperatures above T_{pc} , and discuss some discerning observables which can distinguish between the two. We demonstrate that the onset of localization at high temperatures due to disorder is distinct from the localization driven by topological fluctuations and can only be observed when the $U_A(1)$ subgroup of the chiral symmetry group is *effectively* restored.

We also calculate for the first time the structural rigidity of the Dirac eigenvalues measured in terms of the curvature arising as a result of a twist applied to one of the spatial boundaries of the lattice box. The curvature of the eigenvalues of the Hamiltonian is related to the Thouless conductance [56]. We propose to use the analogue of the Thouless conductance for the Dirac eigenspectrum as a diagnostic tool for characterizing the *effective* restoration of the anomalous $U_A(1)$ subgroup of the chiral symmetry in QCD.

IV. DETAILS ABOUT THE NUMERICAL TECHNIQUES

The gauge configurations for QCD with two light and a strange quark flavor were generated using Möbius domain wall discretization for fermions and Iwasaki gauge action. The computations were performed on a space-time lattice which has $N = 32$ sites along each of the three spatial directions and $N_\tau = 8$ sites along the Euclidean temporal direction. We focused our attention on the high temperature deconfined phase of QCD at temperatures $T = 164-195$ MeV to study the spectral properties of the QCD Dirac operator where the non-singlet part of the (almost) exact two flavor chiral symmetry is *effectively* restored whereas its $U_A(1)$ subgroup remains broken significantly. Some of these gauge configurations for $T \lesssim 181$ MeV were already generated and used for calculating the disconnected piece of the chiral susceptibility [57]. However all the gauge ensembles for $T \gtrsim 195$ MeV were generated from scratch. Details of the parameters used in the configuration generation and the number of eigenvalues computed at each statistically independent configuration at different temperatures are mentioned in Table. I. The quark masses are physical which is fixed by setting the value of the pion mass to 140 MeV and kaon mass to 435 MeV [57]. The temperatures $T = 1/(N_\tau a)$ are calculated at each value of the gauge coupling g relating it to the lattice spacing a through two-loop β -function and then denoted in physical units using the Sommer parameter r_0 . The spatial lattice size in physical units varies between 4-2.5 fm for $T = 195-339$ MeV.

On each of these gauge configurations, we calculate the first 100-200 non-zero eigenvalues of $D_{ov}D_{ov}^\dagger$, where D_{ov} is the massless overlap Dirac operator. This choice of the lattice Dirac operator is motivated by the fact that the overlap fermions have an exact chiral symmetry on the lattice, satisfy an index theorem and do not have additional lattice artifacts due to the breaking of chiral symmetry as in case of Wilson fermions or the breaking of flavor symmetry as for the staggered fermions. We have numerically implemented the overlap Dirac operator by representing the matrix sign function exactly in terms of the first 30 eigenvalues of $D_w^\dagger D_w$ and approximating it by a Zolotarev rational polynomial with 25 terms in the rest of the vector space. The numerical accuracy of our procedure ensures that the resultant overlap Dirac operator satisfies the Ginsparg-Wilson relation to a precision of $\lesssim 10^{-9}$ on each gauge configuration we have studied and the sign function is implemented to a numerical precision of 10^{-10} . The eigenvalues of the overlap Dirac operator are calculated numerically using the Kalkreuter-Simma Ritz algorithm with restarts. For optimization, we have first estimated the number and chirality of zero modes present per configuration by measuring the first 10 eigenvalues of $D_{ov}D_{ov}^\dagger$ and then projected the operator to the opposite chirality sector. We then calculate $\mathcal{O}(100)$ eigenvalues of this overlap Dirac operator projected to one particular chirality and extracted the eigenvalues of

D_{ov} from them. We henceforth denote their imaginary values as λ . We have also checked that the real part of the first $\mathcal{O}(200)$ overlap eigenvalues is about two orders of magnitude smaller, hence sub-dominant compared to its imaginary part. This allows us to directly relate our study to the continuum case where the Dirac operator has only imaginary eigenvalues.

T (MeV)	β	c_5	L_5	N_s	N_τ	N_{eigen}	N_{confs}
164	1.725	1.5	16	32	8	100	95
177	1.771	1.0	16	32	8	100	93
195	1.829	0.9	16	32	8	100	101
270	2.130	0.5	24	32	8	150	86
314	2.250	0.5	12	32	8	200	111
339	2.310	0.5	12	32	8	200	73

Tab. I. Number of gauge configurations studied at different temperatures (corresponding to the values of $\beta = 6/g^2$) and the lattice sizes used in this work. The table also lists the number of overlap Dirac eigenvalues calculated per gauge configuration, along with the values of the Möbius parameter c_5 and L_5 used in the generation of gauge ensembles at each temperature.

We also calculated the correlation between the real part of the renormalized Polyakov loop with these first 100-200 Dirac eigenstates. We performed our calculation using the gradient flow renormalization scheme using the Wilson gauge action. The flow equation is solved using a fourth order Runge-Kutta scheme with a step size of 0.01 up to a flow time t which follows the relation $a \ll \sqrt{8t} \ll 1/T$. To ensure that this criterion is satisfied for all temperatures we have studied, the value of the flow time in physical units was chosen to be $\sqrt{8t} = 0.44$ fm for $T \leq 195$ MeV and $\sqrt{8t} = 0.25$ fm for higher temperatures $T > 200$ MeV. We had to apply a constant shift in free energy to match with the earlier continuum extrapolated results from Ref. [58] in order to fix the scale, which was done at the highest temperature. This same shift in the free energy for two lower temperatures 270 and 314 MeV also gave us an estimate of the renormalized Polyakov loop which is in good agreement with the continuum results in Ref. [58].

V. RESULTS

A. Level spacing ratios near the chiral crossover transition

We first calculate the spacing between the neighboring eigenvalues of the Dirac operator $s_n = \lambda_{n+1} - \lambda_n$ at different temperatures. Instead of constructing the level spacing distribution we study the normalized ratios of the consecutive level spacing distribution defined as $\tilde{r}_n = \min(r_n, 1/r_n)$, where $r_n = s_{n+1}/s_n$, which eliminates the local dependence of spacing distributions on

the eigenvalue level density [59]. Hence it is insensitive to systematic errors that arise while performing the unfolding of the spacing distribution, with limited statistics and in small volumes. We had previously advocated for its use for the first time to study and understand the localization of the eigenstates of QCD Dirac operator [38]. Results of our calculations for $\langle \tilde{r} \rangle$ in bins of λ/T obtained after averaging over gauge configurations are summarized in Fig. 1.

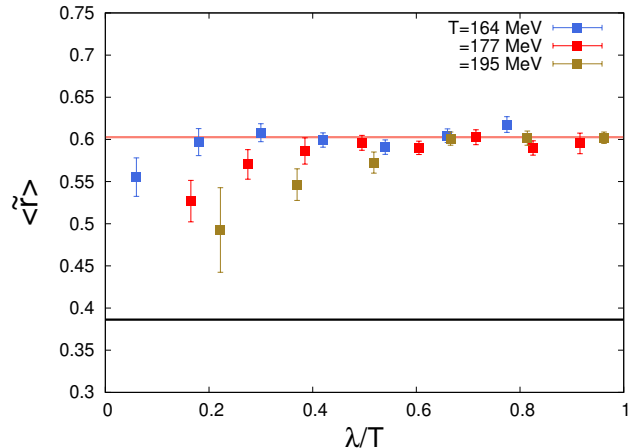


Fig. 1. The variation of $\langle \tilde{r} \rangle$ in the bins of eigenvalues in the temperature range where the non-singlet part of chiral symmetry is *effectively* restored but not its $U_A(1)$ subgroup. The orange and black solid lines represent the expected $\langle \tilde{r} \rangle$ for the GUE and Poisson statistics respectively.

We first focus at $T = 164$ MeV which is above the chiral pseudo-critical temperature. We observe that in lowest bin the value of $\langle \tilde{r} \rangle$ is intermediate between an uncorrelated and a Gaussian Unitary ensemble, we call such modes as *intermediate*. This categorization of modes into *intermediate* and bulk can be easily done from Fig.1. For temperatures $T = 164, 177$ and 195 MeV, all the modes which fall below $\lambda/T = 0.12, 0.33$ and 0.6 respectively are designated as intermediate modes, whereas the ones above these values are identified to be bulk modes. At the lowest temperature the singlet $U_A(1)$ subgroup still remains significantly broken [57] instead only a remnant Z_2 subgroup of the chiral symmetry is intact. The eigenvalues in the smallest bins therefore have different characteristics that distinguish them from the bulk eigenspectrum which has an average value of $\langle \tilde{r} \rangle = 0.602$ consistent with expectations from GUE [38].

In order to provide an interpretation for their properties in terms of universal properties of random matrices, we refer to a recent attempt to understand universal level spacing ratios of random matrices comprising of several independent blocks of known Wigner surmises [60]. Following their construction, we model the average spacing ratio for these *intermediate* eigenvalues as a weighted sum $\langle \tilde{r} \rangle = w\langle \tilde{r} \rangle_1 + (1-w)\langle \tilde{r} \rangle_2$, where $\langle \tilde{r} \rangle_{1,2}$ are the average spacing ratios from one single GUE block and two GUE blocks respectively. Here one GUE block repre-

sents the contribution of the bulk modes only, whereas a random matrix construction with two GUE blocks represents the scenario when the infrared eigenmodes that contribute to the chiral condensate and $U_A(1)$ breaking have admixture with the bulk eigenmodes. We remind here that the bulk eigenmodes survive even at temperatures when different subgroups of chiral symmetry are *effectively* restored. Using the values of $\langle\tilde{r}\rangle = 0.55$ for the *intermediate* eigenmodes at $T = 164$ MeV and $\langle\tilde{r}\rangle_1 = 0.602$ and $\langle\tilde{r}\rangle_2 = 0.3992$ from Ref. [60], we obtain the relative weight of the bulk eigenmodes to be $w = 0.74$. In contrast, the value for $\langle\tilde{r}\rangle$ for the lowest bin at $T = 149$ MeV [38] is consistent with one single GUE block because the $SU_A(2)$ and $U_A(1)$ subgroups of the chiral symmetry are explicitly broken and there are no remnant symmetries that can support the block-like decomposition based on symmetries.

B. Level spacing ratios in the region $T_{pc} < T < T_{U(1)}$

We would now like to address the question of what happens to the level spacing ratio of the *intermediate* eigenmodes in the temperature region when the $U_A(1)$ subgroup of chiral symmetry is broken whereas the non-singlet subgroup is *effectively* restored. In this regime the infrared eigenfunctions exhibit very interesting structural properties. We have earlier showed that at $T \sim 181$ MeV the *intermediate* eigenmodes have fractal-like features and calculated their fractal dimension D_f [38]. It was observed that the median value of $D_f \sim 2.5$ which can be understood from the fact that these eigenmodes have a remnant $O(4)$ symmetry due to the *effective* restoration of the flavor non-singlet $SU_A(2)$ subgroup of the chiral symmetry.

The $U_A(1)$ subgroup should also get *effectively* restored eventually at a certain temperature $T_{U(1)}$, where the density of the smallest eigenvalues of the Dirac operator can be explained as arising due to a gauge background consisting of a dilute gas of instantons [57]. In such a case these eigenvalues should follow a level spacing distribution corresponding to an uncorrelated ensemble [61]. However as long as $U_A(1)$ is not *effectively* restored, these infrared Dirac eigenmodes will have mixing with the remnant tail end of the bulk eigenspectrum resulting in an intermediate level statistics for the infrared eigenvalues. This is already evident in Fig. 1 where the average value $\langle\tilde{r}\rangle$ of the eigenmodes in the deep infrared is decreasing as a function of increasing temperatures in the range $1.1 < T/T_{pc} < 1.2$. At these temperatures when the $U_A(1)$ is not yet *effectively* restored we can model the lowest eigenvalues of the Dirac operator arising out of a matrix with a 2-block structure, one of them representing a matrix belonging to a GUE and the other to an uncorrelated ensemble. We have calculated the level spacing ratios in a 2-block system numerically and compared with our lattice data, the details of which are discussed in Section VD.

C. Level spacing ratios in the region $T > T_{U(1)}$

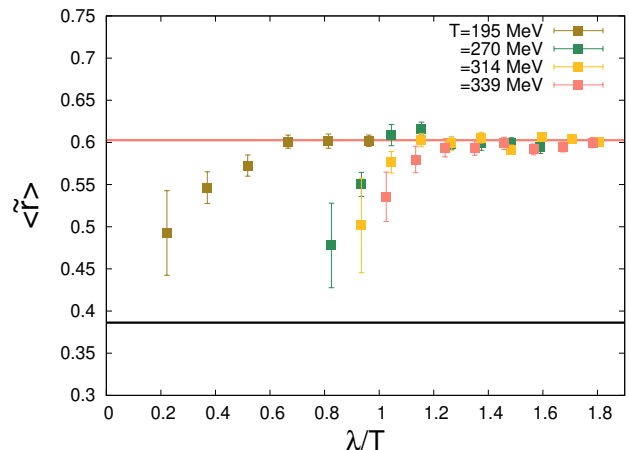


Fig. 2. The variation of $\langle\tilde{r}\rangle$ in small bins in λ/T at high temperatures $T \gtrsim 1.5 T_{pc}$ MeV when the $U_A(1)$ is *effectively* restored compared to the data at 195 MeV.

At even higher temperatures $T > T_{U(1)}$, we expect that Dirac eigenvalues arising due to a gauge background consisting of a dilute gas of instantons will accumulate in the deep infrared part of the eigenvalue spectrum [26, 44], thus separating from the bulk through a gap. We observe this gap opening in the eigenvalue spectrum as the temperatures are increased beyond 195 MeV. This is also evident in our plot for the normalized level ratios for the eigenvalue bins at much higher temperatures $T > 250$ MeV which we have shown in Fig. 2. The eigenvalues $\lambda/T \gtrsim 0.5$ that appear beyond a gap correspond to the region which defines the bulk spectrum for lower temperatures $T \lesssim 200$ MeV. For these eigenmodes the values of $\langle\tilde{r}\rangle$ are also intermediate between the GUE and an uncorrelated matrix ensemble as evident in Fig. 2. Extending the block-like construction discussed in the previous subsection and in section VD, one can interpret the $\langle\tilde{r}\rangle$ in the bins just above the gap arising due to mixing between the chaotic and localized regions present in the bulk spectrum. However the bulk spectrum is overwhelmingly chaotic with a few localized eigenmodes in its tail, resulting in the $\langle\tilde{r}\rangle$ approaching its GUE value immediately within the first few bins as the temperature is increased. This is evidently different from the trend visible in the $\langle\tilde{r}\rangle$ data at $T \lesssim 195$ MeV, which is shown here again in Fig. 2 for the sake of comparison. At this temperature, the gap is negligibly small implying larger fraction of the near-zero eigenmodes contributing to the $\langle\tilde{r}\rangle$, unlike the scenario at $T = 270$ MeV. Anderson-like localization phenomenon for the Dirac spectrum [16, 28, 49] has been studied in the same temperature regime discussed in this section. We provide a more detailed interpretation of our data in section VE and discuss how well it can be compared to the critical eigenfunctions in a 3D Anderson model near the mobility edge [14, 62]. Again, as discussed

in the subsection A, in Fig. 2 we can categorize the eigenspectrum into *intermediate* and bulk modes. We characterize all the modes for which $\lambda/T < 1.0, 1.1$ and 1.2 as *intermediate modes* for temperature $T = 270, 314$ and 339 MeV respectively, whereas modes above these values are characterized as bulk modes. Note that the values of $\langle \tilde{r} \rangle$ in the lowest bin in λ/T at these temperatures are not shown in the plot due to large signal-to-noise ratio related to low statistics.

D. Interpreting the appearance of Dirac eigenvalues with intermediate level statistics

In this section we outline how the normalized level ratios $P(\tilde{r})$, for eigenvalues appearing in the infrared part of the QCD Dirac spectrum can give us important physical insights about their localization properties. Before we proceed we summarize our lattice results for $P(\tilde{r})$ of the different regions of Dirac spectrum labeled as *intermediate* and bulk, as a function of temperature, in the left and right panels of Fig. 3 respectively. The $P(\tilde{r})$ for bulk modes for all the temperatures $T > T_{pc}$ are in excellent agreement with the prediction from random matrices belonging to GUE, as expected. The distribution $P(\tilde{r})$ for the *intermediate* eigenvalues is clearly different both from the expectations of uncorrelated eigenvalues as well as a GUE. The questions we would like to address are what the physical origin of this *intermediate* trend is and how to replicate this in terms of a simple model of random matrices with admixture with uncorrelated eigenvalues. The amount of this admixture, in general, should be a function of temperature. An earlier study with the staggered Dirac spectrum in the continuum limit also observed distinctly different properties of these so-called *intermediate* eigenvalues that proliferate when $SU_A(2)$ is effectively restored compared to the infrared eigenvalues in the chiral symmetry broken phase [34].

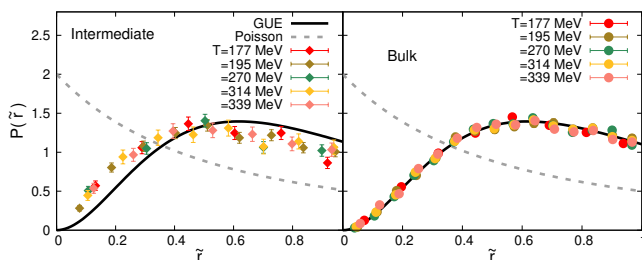


Fig. 3. Probability distribution of \tilde{r} for the intermediate (left) and bulk (right) eigenvalues at different temperatures compared with its values for random matrices belonging to GUE (solid line) and those belonging to uncorrelated eigenvalues following Poissonian level statistics (dotted line).

We follow three different approaches to model the distribution of \tilde{r} for the *intermediate* eigenvalues in the same spirit to but by extending the concepts from random matrix theory. In our first model, we consider a random

matrix belonging to GUE with 0.3 million eigenvalues, the probability distribution $P(\tilde{r})$ for these eigenvalues is well known and expected to follow the GUE prediction, which is shown in Fig. 4 as a black solid line. In the next step we construct a sufficiently small block of eigenvalues drawn from a uniform random distribution with a spacing distribution akin to uncorrelated eigenvalues following Poisson statistics whose size is 3% and 15% of the GUE block respectively. The eigenvalues of this block are chosen such that it lies in-between the range of the eigenvalues present in the GUE block, to allow for a complete mixture of the uncorrelated and GUE eigenvalues without any leakage. This is done to mimic the QCD Dirac spectrum as closely as possible, where we do not observe any localized uncorrelated eigenvalues. Whenever a new eigenvalue is inserted in between existing eigenvalues of the GUE block three new normalized level ratios arise $\tilde{r}_{n_1}, \tilde{r}_{n_2}, \tilde{r}_{n_3}$ due to this insertion. In order to be more explicit, let us assume a new eigenvalue $\lambda_{n'}$ is inserted between the existing GUE eigenvalues λ_n and λ_{n+1} such that the spectrum of the new mixed ensemble is denoted by $\lambda_0, \lambda_1, \dots, \lambda_{n-1}, \lambda_n, \lambda_{n'}, \lambda_{n+1}, \lambda_{n+2}, \dots, \lambda_{N-1}$. Here λ_i , where $i = 0, \dots, N-1$ are eigenvalues of our original GUE-block of size N . The three new level ratios that arise as a result are $r_{n_1} = \frac{\lambda_{n'} - \lambda_n}{\lambda_n - \lambda_{n-1}}$, $r_{n_2} = \frac{\lambda_{n+1} - \lambda_{n'}}{\lambda_{n'} - \lambda_n}$ and $r_{n_3} = \frac{\lambda_{n+2} - \lambda_{n+1}}{\lambda_{n+1} - \lambda_{n'}}$ which are normalized to give $\tilde{r}_{n_i} = \min\left(r_{n_i}, \frac{1}{r_{n_i}}\right)$. The new eigenvalues are accepted only if all three locally induced \tilde{r} are compatible with the target distribution i.e. $P_{\text{GUE}}(\tilde{r})$, implemented through an independent accept-reject criterion. The acceptance criterion of the newly selected eigenvalue is denoted as $\prod_{i=1}^3 \frac{P_{\text{GUE}}(\tilde{r}_{n_i})}{P_{\text{GUE}}^{\text{max}}}$, where $P_{\text{GUE}}(\tilde{r})$ is the probability distribution of \tilde{r} for matrices belonging to GUE whereas $P_{\text{GUE}}^{\text{max}}$ is the maximum value possible for the distribution $P_{\text{GUE}}(\tilde{r})$.

Although the probability with which each new eigenvalue is accepted is same as that of a GUE, for sufficiently small block size of these new eigenvalues it is obvious that these will have a level repulsion consistent with a Poissonian distribution, as there exist no correlations between them. The probability distributions $P(\tilde{r})$ for the eigenvalues in this new block with block sizes 3% and 15% of the GUE-block respectively are shown in Fig. 4. From the plot it is clearly evident that for a smaller block which is 3% of the original GUE-block, the $P(\tilde{r})$ agrees well with that known for a Poisson distribution. In the same figure, we have also shown $P(\tilde{r})$ for the full spectrum where existing eigenvalues from a GUE have a mixture of 3% and 15% of Poissonian eigenvalues labeled as mixed. From the Fig. 4 it is evident that this model cannot explain the intermediate $P(\tilde{r})$ in Fig. 3 for smaller values of \tilde{r} .

Our second model has an approach similar to the first but in this case the new random eigenvalues are accepted within the large GUE-block with acceptance rate of the newly purposed eigenvalue given by $\prod_{i=1}^3 \frac{P_{\text{P}}(\tilde{r}_{n_i})}{P_{\text{P}}^{\text{max}}}$, where $P_{\text{P}}(\tilde{r})$ is the probability distribution of normalized level

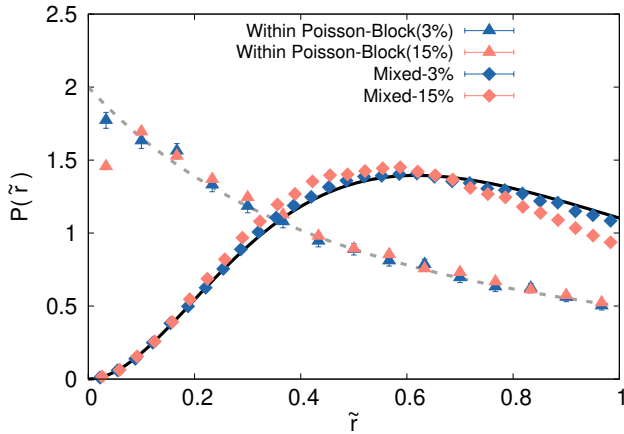


Fig. 4. The probability distribution of the normalized level ratios $P(\tilde{r})$ for our first matrix model where a GUE block is additionally mixed with a block of uncorrelated eigenvalues following level statistics similar to a Poisson distribution selected with a probability distribution weight for \tilde{r} determined from a GUE. The $P(\tilde{r})$ for the newly added uncorrelated block, and the entire mixed matrix are denoted as triangles and diamonds respectively with 3% (blue) and 15% (orange) admixture.

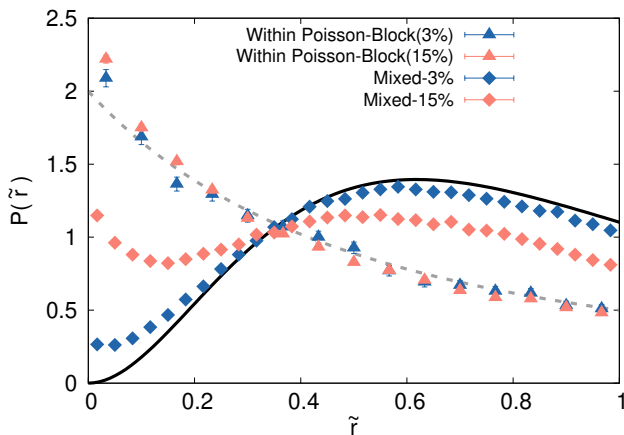


Fig. 5. The $P(\tilde{r})$ for our second matrix model where a GUE block is additionally mixed with a block of uncorrelated eigenvalues selected with a probability distribution weight for \tilde{r} determined from a Poissonian distribution. The $P(\tilde{r})$ for the newly added uncorrelated block, and the entire mixed matrix are denoted as triangles and diamonds respectively with 3% (blue) and 15% (orange) admixture.

ratios \tilde{r} for uncorrelated eigenvalues following Poisson distribution whereas P_P^{\max} is the maximum possible value possible for the distribution $P_P(\tilde{r})$. In this approach, eigenvalues which are closely spaced will be more favored. We show the results of our calculation of $P(\tilde{r})$ in Fig. 5, where the newly added eigenvalues for block of sizes which are 3% and 15% of the original GUE block. The $P(\tilde{r})$ of the newly added eigenvalue block is close to the value expected from uncorrelated eigenvalues. The

$P(\tilde{r})$ of the entire matrix consisting of GUE and Poisson blocks are labeled as *mixed* and are also shown in same figure. For smaller values of \tilde{r} , the $P(\tilde{r})$ lies as intermediate between a Poisson and the GUE values which is quite different from the trend observed for the *intermediate* eigenvalues of the QCD Dirac spectrum at all temperatures, which motivates us to formulate a third approach.

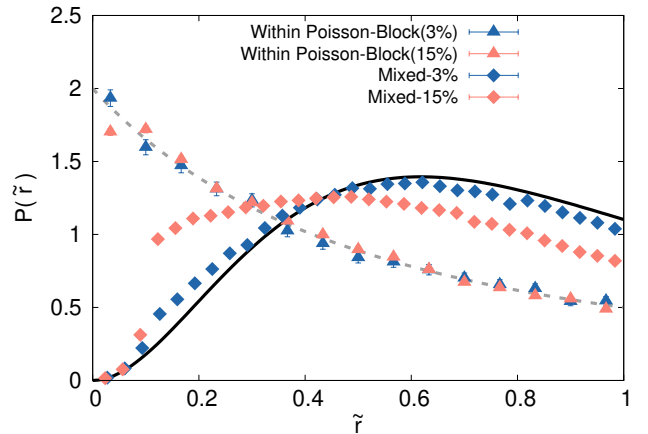


Fig. 6. The $P(\tilde{r})$ for our third matrix model where a GUE block is additionally mixed with a block of uncorrelated eigenvalues selected with a probability distribution weight for \tilde{r} for a mixed distribution (see text for details). The $P(\tilde{r})$ for the newly added uncorrelated block, and the entire mixed matrix are denoted as triangles and diamonds respectively with 3% (blue) and 15% (orange) admixture.

Our third approach will focus on improving the modeling of $P(\tilde{r})$ to more closely mimic the lattice data at smaller values of \tilde{r} . Our lattice data for intermediate eigenvalues shows some enhancement of $P(\tilde{r})$ compared to GUE at moderately small values of \tilde{r} but the probabilities for eigenvalues with very small spacing ratio $\tilde{r} \rightarrow 0$ to occur in the spectrum are heavily disfavored. We model this fact in our random matrix construction by accepting newly generated eigenvalues with a probability $\prod_{i=1}^3 P_{\text{mix}}(\tilde{r}_{n_i})$, where $P_{\text{mix}}(\tilde{r}) \in \left\{ \frac{P_{\text{GUE}}(\tilde{r})}{P_{\text{GUE}}^{\max}}, \frac{P_P(\tilde{r})}{P_P^{\max}} \right\}$, and which of the two elements in this set gets selected depends on the values of $\tilde{r}_{n_1}, \tilde{r}_{n_2}, \tilde{r}_{n_3}$ and a threshold value \tilde{r}_{\max} chosen as $\tilde{r}_{\max} = 0.1$. If values of $\tilde{r}_{n_1}, \tilde{r}_{n_2}, \tilde{r}_{n_3} < 0.1$ then the $P_{\text{mix}}(\tilde{r}_{n_i}) = P_{\text{GUE}}(\tilde{r}_{n_i})$ else $P_{\text{mix}}(\tilde{r}_{n_i}) = P_P(\tilde{r}_{n_i})$, hence this choice explicitly avoids small \tilde{r} . The probability distributions $P(\tilde{r})$ for the newly added eigenvalues constituting a block of size 3% and 15% of the existing GUE block respectively for this hybrid model are shown in Fig. 6. For the smaller block of 3% size of the original GUE-block, the eigenvalue repulsion is consistent with the values obtained with a Poisson distribution. In the same figure, we have also compiled the results for $P(\tilde{r})$ of the entire matrix consisting of both GUE and uncorrelated blocks which we label as *mixed*. The $P(\tilde{r})$ for the eigenvalues in this hybrid approach with an 3-15% admixture can well explain the lattice data for the *in-*

intermediate Dirac eigenvalues. We have also compared the lattice data for $P(\tilde{r})$ at different temperatures between 177-339 MeV with our model 3 predictions, with an $\sim 3 - 15\%$ admixture represented as a band in Fig. 7. This range qualitatively explains the normalized level ratio distribution for this entire range of temperatures that we have studied. Note however that the amount of admixture varies with small intervals in λ/T and its precise determination will require higher statistics in the far infrared part of the spectrum.

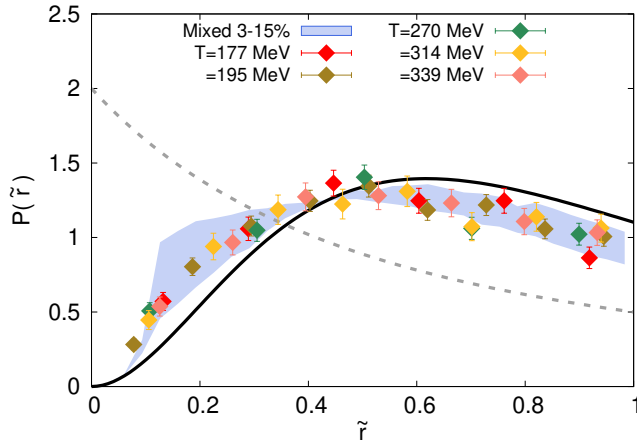


Fig. 7. The probability distribution of \tilde{r} at different temperatures for *intermediate* Dirac eigenmodes compared to the values obtained in our matrix model 3 shown as a blue band. The band represents values of $P(\tilde{r})$ corresponding to 3-15% mixing described within our matrix model 3. The $P(\tilde{r})$ for eigenvalues belonging to uncorrelated and GUE matrices are shown as dashed and solid lines respectively.

We now elaborate on a physical understanding of these models, i.e. why the model 3 can realistically describe the universal level spacing ratios for the *intermediate* Dirac eigenvalues in different temperature regimes. Dyson provided an intuitive understanding [63] of the level spacing distribution of eigenvalues ϵ_i of a $N \times N$ random matrix by modeling them as fictitious Brownian point particles in one dimension at finite temperature whose inverse is the Dyson index β . The potential that describes the Brownian motion of the eigenvalues consists of a confining as well as a repulsive part given by $V(\{\epsilon_i\}) = \sum_{i=1}^N \epsilon_i^2 - \sum_{i < j} \log |\epsilon_i - \epsilon_j|$, where i, j labels the eigenvalues. Performing a Monte-Carlo simulation of this system of N Brownian particles, the distribution of the normalized level spacing ratios of a random matrix belonging to GUE is reproduced.

Now, in order to understand the origin of *intermediate* level statistics in terms of Dyson's construction, we replace the harmonic oscillator potential with one which causes a weaker confinement [64, 65]. The choice of different weak confining potentials was originally motivated in order to construct different classes of random matrix ensembles which have multi-fractal eigenfunctions and to understand what characteristic signa-

tures of such multifractality are inherent in the spacing distribution [65]. For one such choice of a confining potential, $V(\{\epsilon_i\}) = A \sum_i \ln^2 |\epsilon_i|$, we obtain a normalized level spacing ratio distribution which can explain our lattice data for the *intermediate* Dirac eigenvalues, shown in Fig. 8. Though in our calculation we have chosen $A = 0.2$ however we have verified that level spacing ratio distributions are independent of the choice of the strength of the potential A by sufficiently varying it $\in [0, 10]$. Another different choice of a weaker confining potential, e.g. [64], $V(\{\epsilon_i\}) = A \sum_i |\epsilon_i|^\alpha$ can explain our lattice data consistently as well.

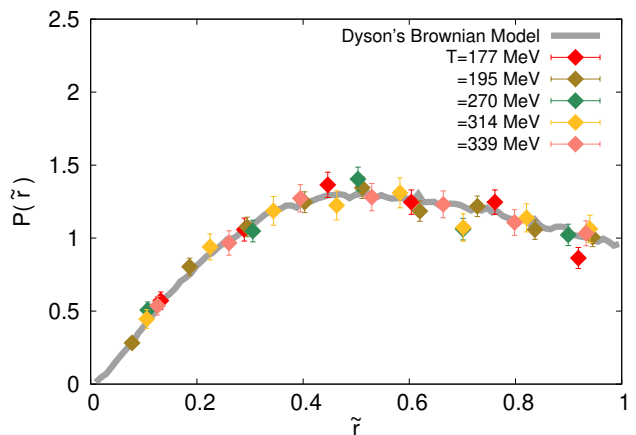


Fig. 8. The probability distribution for \tilde{r} obtained using Dyson's Brownian model for eigenvalues $\{\epsilon_i\}$ moving in presence of a weak confining potential along with a log-repulsion between them shown as a solid line. The probability distributions for the *intermediate* Dirac eigenvalues at different temperatures are shown (as points) for comparison.

We summarize here our attempt to understand the onset of *intermediate* region starting from the predominantly chaotic eigenvalues in the bulk and quantify their level ratios. By varying the fractional admixture of uncorrelated eigenvalues introduced within a GUE matrix block according to a very specific criterion discussed above in model 3, the magnitude of $\langle \tilde{r} \rangle$ for infrared QCD Dirac eigenvalues which start to deviate from GUE can be very well understood. Compared to $T = 195$ the $\langle \tilde{r} \rangle$ at $T = 314$ MeV deviates from the bulk more dramatically within a span of few bins while moving towards the infrared. This information gives us interesting clues about the possible physical origin of the *intermediate* statistics. At temperatures $T < T_{U(1)}$ when the singlet subgroup of chiral symmetry is not *effectively* restored, the amount of admixture gradually increases as we move towards the infrared bins. In the lowest bin, the average value of $\langle \tilde{r} \rangle$ tends to be successively closer to an uncorrelated distribution as temperature is increased to $T_{U(1)}$ when there should be an efficient separation of the near-zero from the bulk eigenvalues [34]. At temperatures $T > T_{U(1)}$, the admixture occurs in a region of comparatively larger eigenvalues, which defined the chaotic bulk for lower tem-

peratures alluding to the fact that the microscopic origin of these uncorrelated eigenvalues is different from that for $T \lesssim T_{U(1)}$.

Similar analysis for the distribution of level ratios have been performed on mixed ensemble of Poisson-GOE matrices in Ref. [66] by generalizing the techniques formulated in Ref. [60] for understanding mixing between eigenvalues of matrices belonging to different symmetry classes [67]. These works [60, 66] derive the joint distribution of consecutive nearest-neighbor level spacings of a compound spectrum constructed out of several spectra with different distribution. However for a Poisson-GUE system there is no analytic solution of the normalized level spacing ratios in this approach, which have to be determined numerically. Our numerical approach is another different way to explain a mixed ensemble of matrices of two symmetry categories. We also note that modeling a mixed level spacing distribution has also been discussed in the literature heuristically as the best fit function with few parameters [68]. A microscopic model consisting of a two-dimensional matrix mimicking a Poisson process weakly coupled with a random matrix belonging to different Wigner surmise [69–71] has also been discussed to fit a mixed distribution in terms of a single parameter that denotes the strength of the coupling.

E. Understanding the origin of disorder and (de)localization in QCD Dirac eigenstates

Having interpreted the Dirac eigenvalues with *intermediate* level statistics as arising due to admixture between eigenvalues with universal level spacing fluctuations of GUE and Poisson type, now we would like to understand what the microscopic origin of such different distribution types and their mixing is.

We recall that in the Euclidean formalism the partition function of QCD can be realized as a path integral with fermion fields satisfying anti-periodic boundary conditions along the compact imaginary time of extent $1/T$. As a result the lowest eigenvalue of the Euclidean lattice Dirac operator is $\sin(\pi/N_\tau)$. Turning on gauge interactions, the temporal part of the Dirac operator can be diagonalized in the limit of weak coupling in terms of diagonal elements at each lattice site which depends on the lowest Matsubara mode shifted by the local Polyakov loop values [71]. A random matrix model of these local Matsubara modes with nearest neighbor interactions closely resembles the tight binding Anderson model [71]. At high temperatures the fluctuations of the Polyakov loop around its mean become rarer and occur at random spatial locations [28, 72, 73], justifying its similarity with a random disorder. However the validity of these assumptions needs to be revisited for temperatures $T_{pc} < T < T_{U(1)}$.

In the regime $T \gtrsim T_{pc}$ there are regions of strong fluctuations in the local values of Polyakov loop which has been demonstrated to be anti-correlated with the prob-

ability density for the occurrence of instanton-dyons [74] which form a semi-classical gas [75, 76]. Hence the origin of disorder at temperatures T_{pc} is largely driven by fluctuations about the topological vacuum in QCD and is very different from a random uncorrelated distribution since the temperature dependence of the topological susceptibility is very different from a dilute instanton gas [41]. This is the same region where $U_A(1)$ remains badly broken precisely because of this non-trivial dependence of the topological fluctuations. When temperatures are increased to say $1.5 T_{pc}$ where the holonomy is trivial, the sites with discernible random fluctuations of the (ensemble-averaged) Polyakov loop values are no longer correlated with the fluctuations of the topological vacuum in QCD. Incidentally this is the regime when $U_A(1)$ is believed to be *effectively* restored which is understood in terms of an onset of dilute instanton gas description of the topological fluctuations. The randomness in the gauge field background is solely driven by the inherent chaotic nature of classical color fluctuations at high temperatures [77, 78].

We also review the literature to clarify some important points which are not often discussed in the context of QCD. Since the gauge field background represents a strongly interacting many-body system at $T_{pc} < T < T_{U(1)}$ it is not clear a priori whether the noise inherent in it can be considered as random as required in an Anderson model. The generalization of Anderson localization in interacting systems, known as many-body localization [79] has been discussed as a finite temperature phase transition and is being currently under intensive review [8, 80]. The characteristic signatures of a (de)localization transition in such interacting systems have been shown to be manifest in different single particle observables [81]. Furthermore, the disorder inherent in the gauge fields in QCD is not quenched (static) but dynamically generated due to self interactions similar to the scenario discussed in the context of interacting lattice spins models [82].

Second, we would like to remind here that when we calculate the eigenvectors of the Dirac operator in presence of a noisy gauge background, we are solving for relativistic single particle states. This is different from a conventional Anderson model which discusses non-relativistic free electrons in presence of a quenched random potential. Anderson transition has been studied in three-dimensional non-interacting Dirac semimetals in presence of quenched disorder [83]. It was reported that such systems have three distinct ground states, i.e. an incompressible semimetal, a compressible diffusive metal, and an insulator, which is in contrast to a conventional Anderson model that describes a transition between only the latter two phases. In presence of a small amount of disorder, there is a quantum phase transition from a semimetal to a dirty metal phase which, on increasing disorder strength, goes over to an insulating phase through the conventional Anderson transition. At very strong disorder one would thus be just probing the semimetal-

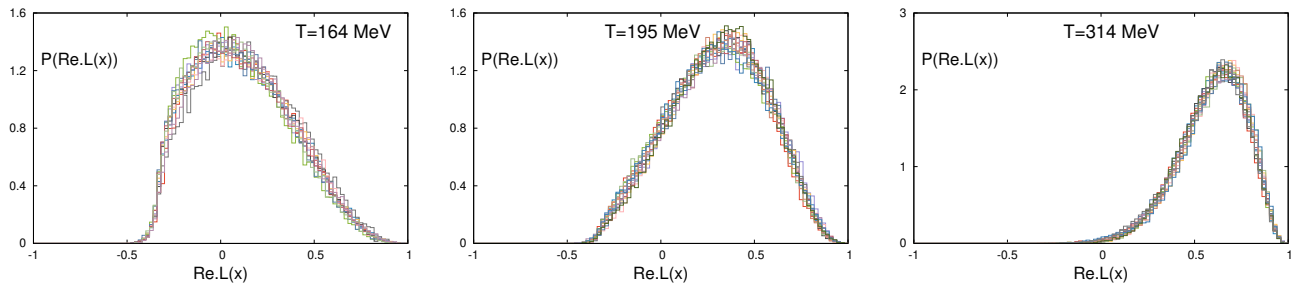


Fig. 9. Probability distribution of the $\text{Re}.P(\mathbf{x})$ for independent gauge configurations, calculated after performing Wilson flow renormalization at three different temperatures above the chiral crossover transition.

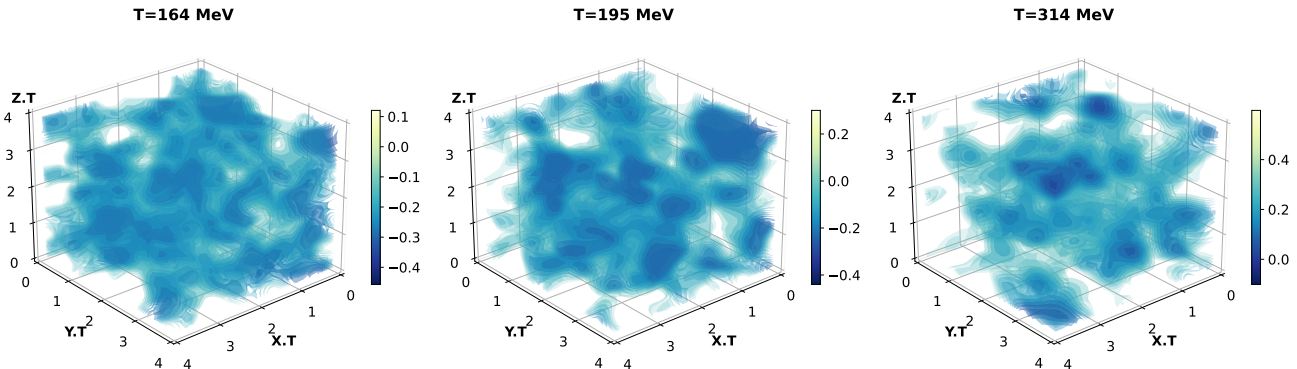


Fig. 10. Visual representation of the local fluctuations of the real part of the Polyakov loop $\text{Re}.P(\mathbf{x})$ which are below its mean value at three different temperatures which are obtained after performing Wilson flow renormalization in a typical configuration. The lightest color in the palette represents its mean value in that particular gauge configuration.

insulator transition. Hence it is also imperative that we have a quantitative estimate of the amount of disorder inherent in the gauge fields in the context of QCD.

We will now discuss here if the presence of *intermediate* eigenvalues in the temperature regime $T > T_{U(1)}$ is intimately correlated with the disorder inherent in the gauge fields, which is typically understood in terms of the fluctuations around the average renormalized Polyakov loop values [72] at each spatial position. We also study how the typical magnitude of these fluctuations varies as a function of temperature and whether these can be still modeled as random uncorrelated sources of localizing potential as required within the Anderson model in the temperature regime $T_{pc} < T < T_{U(1)}$.

The renormalized Polyakov loop has been measured at each spatial site at different temperatures, after performing gradient flow, details of which are mentioned in Sec. IV. We show the probability distribution of renormalized values of the real part of Polyakov loop value at each site \mathbf{x} denoted as of $\text{Re}.P(\mathbf{x})$ for each gauge configuration at different temperatures superposed together in Fig. 9. We observe that the width of the distribution of the renormalized local Polyakov loop values is decreasing with increasing temperatures, demonstrating that the gauge fields are smoother at higher temperatures. Due to the larger width of the distribution at $T \leq 195$ MeV, the

confining wells defined at locations in space for which the real part of the renormalized Polyakov loop values are lower than its average have strong overlap with each other. This is also evident in the density plots of the local fluctuations of the Polyakov loop which are lower than its mean value at each temperature, shown in Fig. 10. At higher temperatures $T = 314$ MeV the large negative fluctuations in $\text{Re}.P(\mathbf{x})$ about its average value become rarer, resulting in a clear separation among these potential wells which are located at random sites. In contrast, close to the crossover transition at $T = 164$ MeV the fluctuations in the renormalized values of Polyakov loop are much more frequent and correlated.

In order to quantify how well these deep negative fluctuations of the renormalized Polyakov loop $\text{Re}.P(\mathbf{x})$ about its mean are correlated with the Dirac eigenstates at each temperature, we calculate the quantity $C_n = \sum_{\mathbf{x}} |\Psi_n(\mathbf{x})|^2 [\text{Re}.P(\mathbf{x}) - \langle \text{Re}.P(\mathbf{x}) \rangle]$. Here $\Psi_n(\mathbf{x})$ is the n^{th} eigenstate of the overlap Dirac operator and its norm at each spatial site \mathbf{x} on the lattice is obtained by integrating out the four-dimensional eigendensity along the temporal direction τ denoted as $|\Psi_n(\mathbf{x})|^2 = \sum_{\tau=0}^{N_\tau-1} |\psi_n(\mathbf{x}, \tau)|^2$. We calculate the net correlation $C(\lambda/T)$ by performing a binning of the C_n for each eigenstate in small bins in λ/T and performing an average over the gauge configurations for different temperatures,

results of which are compiled in Fig. 11. From the figure, it is evident that at higher temperatures $T > 250$ MeV the eigenvalues in the *intermediate* region of the Dirac spectrum are more correlated with the wells of fluctuating renormalized Polyakov loops as compared to temperatures $T \leq 195$ MeV. This demonstrates that indeed the fluctuations in $\text{Re}P(\mathbf{x})$ acts as a random disordered confining potential for these low eigenmodes, however we need to verify this on a larger volume. At $T \leq 195$ MeV, the correlation between the intermediate Dirac eigenstates with the Polyakov loop fluctuations is weaker compared to temperatures $T > 250$ MeV. This is due to the fact that these well-like fluctuations at different lattice sites are no longer rare events; on the contrary they are strongly correlated as observed in Fig. 9. As a result, the *intermediate* eigenstates are largely delocalized over several such locations. This was also evident from the fractal-like behavior of these *intermediate* eigenstates at $T < T_{U(1)}$ in previous works [37, 38]. The values of $C(\lambda/T)$ approaches towards zero for the bulk eigenstates, as expected, since these are delocalized chaotic states that do not feel these tiny fluctuations.

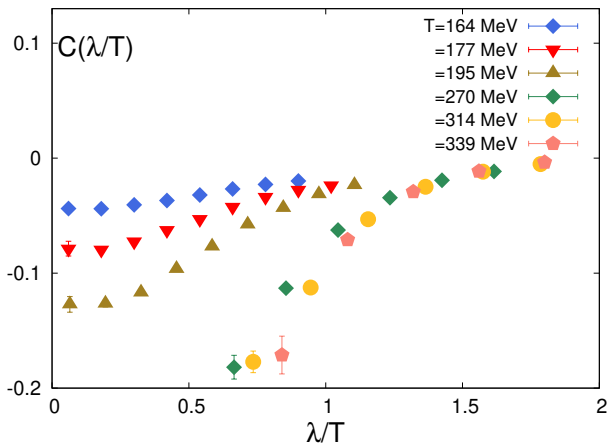


Fig. 11. The correlation $C(\lambda/T)$ between the local density of the Dirac eigenstate and the local fluctuations of $\text{Re}P(\mathbf{x})$ about its mean calculated in small bins of λ/T at different temperatures.

F. Structural features of the Dirac eigenfunctions: Thouless conductance

Apart from the local correlations that are observed for e.g., in the spacing ratios, it is also important to identify global correlations that exist among eigenvalues. This will allow us to identify the physical origin of correlations that result in distinct structural changes in the eigenfunctions of the Dirac operator as a function of temperature.

One such quantity sensitive to global correlations is the Thouless conductance which is measured in terms of the average shift in the eigenvalues of the Hamiltonian of a quantum system when a twist is applied to the

eigenstates along one of the spatial directions of size L , normalized by the average nearest neighbor level spacing s [56]. According to the Thouless criterion, one could then categorize them as extended states if the average shift is much larger than the average level spacing or localized in the opposite limit. In this work however we will discuss the change in the properties of the Dirac eigenvalues when the corresponding eigenfunctions ψ_i are subject to a twist along any of the spatial directions denoted as $\psi_i(x+L) = \psi_i(x)e^{i\eta}$. The eigenvalues λ_i which are sensitive to the twist should acquire a curvature as a result, which we denote as K_i defined as $K_i = |\frac{\partial^2 \lambda_i}{\partial \eta^2}|$. We then calculate the probability distribution of curvature values $P(K)$ of the intermediate and bulk modes separately, acquired due to a sufficiently small twist $\eta = 0.005$. This is performed by choosing appropriate bins in terms of the normalized curvature values $K_i \rightarrow K_i/\langle K \rangle$ obtained by dividing with the average value for intermediate and bulk modes, respectively. After performing an ensemble average on the gauge configurations, the results obtained for $P(K)$ are shown as a function of four different temperatures in Fig. 12.

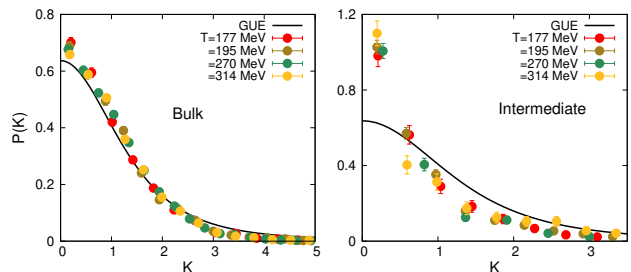


Fig. 12. The curvature distribution of the bulk (left) and intermediate Dirac eigenmodes (right) as a function of temperature. The black solid line represents the expected probability distribution for the curvature K in random matrices belonging to a GUE.

The distribution of the curvature values are consistent with prior expectations from our earlier study [38] and also studies performed in Hamiltonian systems in spin models, for e.g., in the original work of Thouless [56]. Eigenvalues that are delocalized acquire larger curvature upon applying a twist whereas eigenvalues at the infrared edge of the spectrum have a tiny deviation upon twisting. We would like to remind the readers that majority of the intermediate eigenstates are delocalized but not ergodic, their inverse participation ratios do not scale with the spatial volume hence these should mildly depend on the twist at the boundaries of the lattice box, and if at all, will acquire a small curvature. There can be however rare large fluctuations in the curvature distribution due to localized modes which might be situated close to the boundary of the lattice box. Our lattice data for the curvature distribution of the intermediate eigenmodes, shown in the right panel of Fig. 12, are consistent with these expectations. On the other hand, delocalized bulk eigenstates whose inverse participation ratios

exhibit volume scaling as $\sim L^{-2.8}$ [38] should be most sensitive to the applied twist. In order to quantify how close these bulk eigenstates are to GUE predictions, we compare their curvature distribution with those of the eigenvalues of random matrices belonging to GUE [84], given as $P(K) = \frac{2}{\pi} \frac{1}{(K^2+1)^2}$. As evident from Fig. 12 there is a fairly good agreement of the $P(K)$ for bulk eigenmodes with the prediction from a GUE, at different temperatures.

We next calculate the Thouless conductance constructed out of Dirac eigenstates, defined as $g_{\text{Th}} = \frac{1}{\langle s \rangle} \langle K_i \rangle_{\eta \rightarrow 0}$ in terms of the curvature K_i acquired by the i -th eigenstate subject to an infinitesimally small twist $\eta \rightarrow 0$, which in our case is $\eta = 0.005$. Calculating the averages of the curvatures $\langle K_i \rangle$ and level spacings $\langle s \rangle$ in small bins in λ/T for three different temperatures, we summarize our results for g_{Th} in Fig. 13. The magnitude of g_{Th} is not insignificantly small for the bin in the *intermediate* region, which implies that these eigenstates are not exponentially localized. The values of g_{Th} increase with increasing values of λ/T . Performing a fit to the data for the bulk eigenvalues with a linear in λ ansatz, shown as dashed lines in Fig. 13, we obtain a positive slope $dg_{\text{Th}}(\lambda/T)/d(\lambda/T)$ for four different temperatures which are mentioned in the legend of the same plot and we also observe from the slope value that there is a faster rise in conductance with temperature from the bulk eigenmodes. The initial growth in the value of the Thouless conductance as a function of λ/T in the bins containing *intermediate* eigenvalues is faster compared to a linear rise for the bulk modes. Thus g_{Th} allows us to unambiguously disentangle the bulk eigenvalues from the rest.

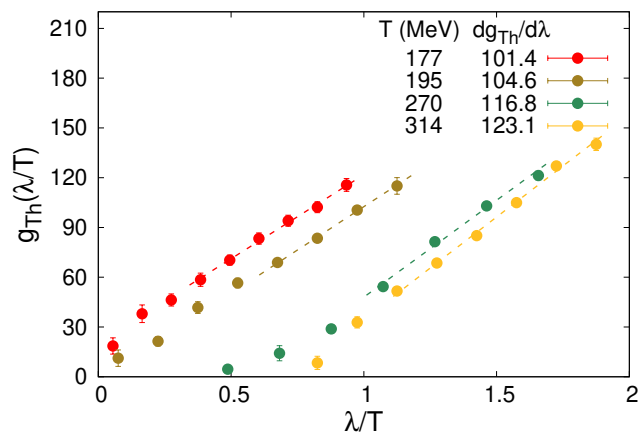


Fig. 13. The Thouless conductance for different eigenvalue bins calculated at temperatures $T = 177, 195, 270, 314$ MeV respectively. The dashed line represents a linear fit to the g_{Th} for bulk eigenmodes and the corresponding slopes $\frac{dg_{\text{Th}}(\lambda/T)}{d(\lambda/T)}$ are mentioned in the legend.

Next, we focus only on the lowest few *intermediate* eigenvalues which feel similar correlation quantified in

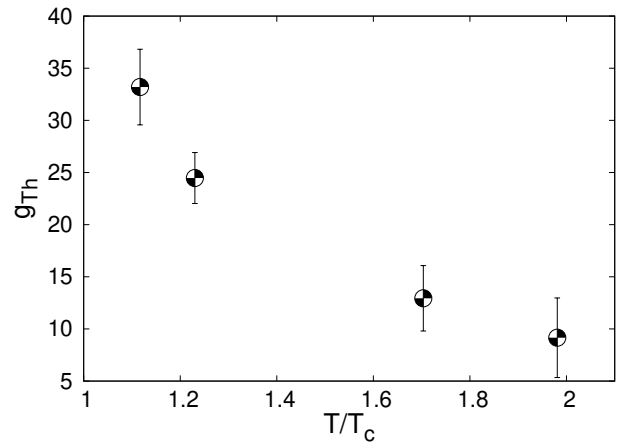


Fig. 14. Thouless conductance for the smallest eigenmodes chosen such that these have similar values of $C(\lambda/T)$, shown as a function of temperature.

terms of $C(\lambda/T)$. The results of Thouless conductance for these *intermediate* eigenmodes as a function of temperature are shown in Fig. 14. It is clear that with increasing temperature these low eigenmodes contribute to provide a small value of the Thouless conductance as expected as these eigenstates are well localized within the wells formed due to fluctuations in the $\text{Re}.P(\mathbf{x})$. The error on the estimate of g_{Th} is quite large at the highest temperature due to insufficient number of eigenmodes in the lowest bins and finite-volume effects. From the temperature dependence of g_{Th} , it can be potentially used to mimic as an *order parameter* for the restoration of $U_A(1)$. Since $U_A(1)$ is not an exact symmetry, one cannot construct an order parameter that conventionally characterizes a thermal phase transition. Instead, we suggest that the effects of $U_A(1)$ breaking and restoration should be inferred from the change in the geometric (structural) properties of the eigenvalues, which are manifest in quantities like g_{Th} .

VI. SUMMARY AND OUTLOOK

In this work, we have performed a detailed study of the properties of the infrared eigenstates of the massless Dirac operator on thermal gauge ensembles, in order to study properties in a strongly correlated system described by QCD. We particularly focused on the question of how can we study the *effective* restoration of (the anomalous) $U(1)$ subgroup of chiral symmetry using the spectral and structural properties of the Dirac eigenstates and what the consequences of the restoration are. We have performed these calculations with an extensive set of gauge configurations generated using Möbius domain wall fermion discretization, over a range of temperatures up to $\sim 2 T_{pc}$. Using normalized level spacing ratios we have unambiguously identified those eigenvalues which have *intermediate* level statistics from the overwhelm-

ing majority of the bulk eigenvalues that have level repulsions consistent with random matrices belonging to a GUE. Though we previously provided an explanation of the existence of these *intermediate* eigenstates just above T_{pc} as arising due to the restoration of the non-singlet part of the almost exact chiral symmetry for QCD with two light quark flavors [38], however their persistence at very high temperature has a different physical origin.

By studying the correlation of these *intermediate* eigenstates with the fluctuations of the real part of the renormalized Polyakov loop about its average, we could clearly show their distinct physical properties at high temperatures $T > 250$ MeV, where the axial U(1) symmetry is expected to be effectively restored compared to $T < 200$ MeV where it remains broken. In fact the density plots for the real part of the renormalized Polyakov loop reveal that at $T > 250$ MeV, there are deep localized fluctuations at random sites of the lattice which are uncorrelated with each other mimicking random disorder as discussed in the context of Anderson model of electrons. We will need better control over the finite volume effects to understand whether these infrared eigenstates with *intermediate* level ratios describe the physics near the mobility edge in an Anderson-like transition. We aim to address this issue in a future study. We also showed that the fluctuations in the real part of the renormalized Polyakov loop are more correlated at $T < 200$ MeV, quite unlike the original proposal of a random disorder by Anderson. Our study hints to the fact that the signatures of a (de)-localization transition will start to become more prominent when the axial U(1) subgroup of chiral symmetry is effectively restored.

We then provide an explanation for the existence of these Dirac eigenstates with *intermediate* level statistics within a matrix model. By introducing additional uncorrelated eigenvalues within a large random matrix belonging to a GUE with a very specific accept/reject criterion, we showed that the normalized level ratios of this en-

larged matrix, could beautifully explain the *intermediate* level ratios of the QCD Dirac eigenvalues shown in Fig.7. We also discussed an intuitive understanding of such a matrix model construction in terms of Brownian motion model of eigenvalues. Unlike the eigenvalues of a random matrix belonging to a GUE whose level separations arise due to its Brownian motion in a thermal bath with a weak log-repulsion and a strong confining harmonic potential, the intermediate eigen level ratios can be explained if the confining potential is weakened.

We also for the first time calculate the analogue of the Thouless conductance g_{Th} due to the Dirac eigenstates which quantifies the structural rigidity of the different eigenstates due to a twist applied along one of the spatial boundaries of the lattice box. We use the curvature distribution and the g_{Th} to also independently distinguish the *intermediate* eigenstates from the bulk ones. Calculating the g_{Th} for the *intermediate* eigenstates that are strongly correlated with the Polyakov loop fluctuations, we demonstrate its gradual decrease as a function of temperature. The point of inflection of this curve could give us an estimate of the temperature where axial U(1) is *effectively* restored, and we will study this observable at larger volumes to firmly establish our claim in a future study.

VII. ACKNOWLEDGMENTS

We are grateful to Robin Kehr and Lorenz von Smekal for discussions on related topics during the course of this work. The authors acknowledge the use of High Performance Computing resources at the Institute of Mathematical Sciences. Our GPU code is in part based on some of the publicly available QUDA [85] and Grid Python Toolkit [86] libraries.

-
- [1] O. Bohigas, M. J. Giannoni, and C. Schmit, Phys. Rev. Lett. **52**, 1 (1984).
 - [2] M. V. Berry and M. Tabor, Proceedings of the Royal Society of London. A. Mathematical and Physical Sciences **356**, 375 (1977).
 - [3] J. M. Deutsch, Rept. Prog. Phys. **81**, 082001 (2018), arXiv:1805.01616 [quant-ph].
 - [4] O. Bohigas, S. Tomsovic, and D. Ullmo, Phys. Rept. **223**, 43 (1993).
 - [5] M. V. Berry and M. Robnik, Journal of Physics A: Mathematical and General **17**, 2413 (1984).
 - [6] T. Prosen and M. Robnik, Journal of Physics A: Mathematical and General **27**, 8059 (1994).
 - [7] S. H. Tekur, S. Kumar, and M. S. Santhanam, Phys. Rev. E **97**, 062212 (2018).
 - [8] R. Nandkishore and D. A. Huse, Ann. Rev. Condensed Matter Phys. **6**, 15 (2015), arXiv:1404.0686 [cond-mat.stat-mech].
 - [9] M. Serbyn and J. E. Moore, Phys. Rev. B **93**, 041424 (2016), arXiv:1508.07293 [cond-mat.dis-nn].
 - [10] M. Amini, E. Cuevas, I. M. Khaymovich, and V. E. Kravtsov, New J. Phys. **17**, 122002 (2015).
 - [11] S. Moudgalya and O. I. Motrunich, Phys. Rev. X **12**, 011050 (2022), arXiv:2108.10324 [cond-mat.stat-mech].
 - [12] S. Moudgalya, B. A. Bernevig, and N. Regnault, Rept. Prog. Phys. **85**, 086501 (2022), arXiv:2109.00548 [cond-mat.str-el].
 - [13] D. Adler, D. Wei, M. Will, K. Srakaew, S. Agrawal, P. Weckesser, R. Moessner, F. Pollmann, I. Bloch, and J. Zeiher, Nature **636**, 80 (2024), arXiv:2404.14896 [cond-mat.quant-gas].
 - [14] B. I. Shklovskii, B. Shapiro, B. R. Sears, P. Lambrianides, and H. B. Shore, Phys. Rev. B **47**, 11487 (1993).
 - [15] P. W. Anderson, Phys. Rev. **109**, 1492 (1958).
 - [16] M. Giordano and T. G. Kovacs, Universe **7**, 194 (2021), arXiv:2104.14388 [hep-lat].

- [17] S. Sharma, PoS **CPOD2017**, 086 (2018).
- [18] M. P. Lombardo and A. Trunin, *Int. J. Mod. Phys. A* **35**, 2030010 (2020), arXiv:2005.06547 [hep-lat].
- [19] A. Bazavov *et al.* (HotQCD), *Phys. Lett. B* **795**, 15 (2019), arXiv:1812.08235 [hep-lat].
- [20] F. Burger, E.-M. Ilgenfritz, M. P. Lombardo, and A. Trunin, *Phys. Rev. D* **98**, 094501 (2018), arXiv:1805.06001 [hep-lat].
- [21] S. Borsanyi, Z. Fodor, J. N. Guenther, R. Kara, S. D. Katz, P. Parotto, A. Pasztor, C. Ratti, and K. K. Szabo, *Phys. Rev. Lett.* **125**, 052001 (2020), arXiv:2002.02821 [hep-lat].
- [22] J. J. M. Verbaarschot, *Phys. Rev. Lett.* **72**, 2531 (1994), arXiv:hep-th/9401059.
- [23] J. J. M. Verbaarschot and I. Zahed, *Phys. Rev. Lett.* **70**, 3852 (1993), arXiv:hep-th/9303012.
- [24] J. J. M. Verbaarschot, *Nucl. Phys. B Proc. Suppl.* **53**, 88 (1997), arXiv:hep-lat/9607086.
- [25] T. Kanazawa and M. Kieburg, *J. Phys. A* **51**, 345202 (2018), arXiv:1804.03985 [math-ph].
- [26] V. Dick, F. Karsch, E. Laermann, S. Mukherjee, and S. Sharma, *Phys. Rev. D* **91**, 094504 (2015), arXiv:1502.06190 [hep-lat].
- [27] S. Sharma, V. Dick, F. Karsch, E. Laermann, and S. Mukherjee, *Nucl. Phys. A* **956**, 793 (2016), arXiv:1602.02197 [hep-lat].
- [28] L. Holicki, E.-M. Ilgenfritz, and L. von Smekal, PoS **LATTICE2018**, 180 (2018), arXiv:1810.01130 [hep-lat].
- [29] A. Tomiya, G. Cossu, S. Aoki, H. Fukaya, S. Hashimoto, T. Kaneko, and J. Noaki, *Phys. Rev. D* **96**, 034509 (2017), [Addendum: *Phys. Rev. D* **96**, 079902 (2017)], arXiv:1612.01908 [hep-lat].
- [30] S. Aoki, Y. Aoki, G. Cossu, H. Fukaya, S. Hashimoto, T. Kaneko, C. Rohrhofer, and K. Suzuki (JLQCD), *Phys. Rev. D* **103**, 074506 (2021), arXiv:2011.01499 [hep-lat].
- [31] S. Aoki, Y. Aoki, H. Fukaya, S. Hashimoto, C. Rohrhofer, and K. Suzuki (JLQCD), *PTEP* **2022**, 023B05 (2022), arXiv:2103.05954 [hep-lat].
- [32] T.-W. Chiu, PoS **LATTICE 2013**, 165 (2014).
- [33] M. I. Buchoff *et al.*, *Phys. Rev. D* **89**, 054514 (2014), arXiv:1309.4149 [hep-lat].
- [34] O. Kaczmarek, R. Shanker, and S. Sharma, *Phys. Rev. D* **108**, 094501 (2023), arXiv:2301.11610 [hep-lat].
- [35] A. Alexandru and I. Horváth, *Phys. Rev. Lett.* **127**, 052303 (2021), arXiv:2103.05607 [hep-lat].
- [36] A. Alexandru, I. Horváth, and N. Bhattacharyya, *Phys. Rev. D* **109**, 014501 (2024), arXiv:2310.03621 [hep-lat].
- [37] A. Alexandru, C. Bonanno, M. D'Elia, and I. Horváth, (2024), arXiv:2404.12298 [hep-lat].
- [38] H. Pandey, R. Shanker, and S. Sharma, (2024), arXiv:2407.09253 [hep-lat].
- [39] A. Alexandru and I. Horváth, *Phys. Rev. D* **92**, 045038 (2015), arXiv:1502.07732 [hep-lat].
- [40] A. Alexandru and I. Horváth, *Phys. Rev. D* **100**, 094507 (2019), arXiv:1906.08047 [hep-lat].
- [41] P. Petreczky, H.-P. Schadler, and S. Sharma, *Phys. Lett. B* **762**, 498 (2016), arXiv:1606.03145 [hep-lat].
- [42] R. Bignell, G. Aarts, C. Allton, B. Jäger, S. Kim, J.-I. Skullerud, and A. Smecca, in *42th International Symposium on Lattice Field Theory* (2026) arXiv:2601.21178 [hep-lat].
- [43] T.-W. Chiu and T.-H. Hsieh, (2026), arXiv:2602.14811 [hep-lat].
- [44] H. T. Ding, S. T. Li, S. Mukherjee, A. Tomiya, X. D. Wang, and Y. Zhang, *Phys. Rev. Lett.* **126**, 082001 (2021), arXiv:2010.14836 [hep-lat].
- [45] T. G. Kovacs, *Phys. Rev. Lett.* **132**, 131902 (2024), arXiv:2311.04208 [hep-lat].
- [46] S. Borsanyi *et al.*, *Nature* **539**, 69 (2016), arXiv:1606.07494 [hep-lat].
- [47] C. Bonati, M. D'Elia, G. Martinelli, F. Negro, F. Sanfilippo, and A. Todaro, *JHEP* **11**, 170 (2018), arXiv:1807.07954 [hep-lat].
- [48] M. Giordano, S. D. Katz, T. G. Kovacs, and F. Pittler, *JHEP* **02**, 055 (2017), arXiv:1611.03284 [hep-lat].
- [49] R. Kehr, D. Smith, and L. von Smekal, (2023), arXiv:2304.13617 [hep-lat].
- [50] A. M. Garcia-Garcia and J. C. Osborn, *Phys. Rev. D* **75**, 034503 (2007), arXiv:hep-lat/0611019.
- [51] T. G. Kovacs and F. Pittler, *Phys. Rev. Lett.* **105**, 192001 (2010), arXiv:1006.1205 [hep-lat].
- [52] M. Giordano, T. G. Kovacs, and F. Pittler, *Phys. Rev. Lett.* **112**, 102002 (2014), arXiv:1312.1179 [hep-lat].
- [53] L. Ujfalusi, M. Giordano, F. Pittler, T. G. Kovács, and I. Varga, *Phys. Rev. D* **92**, 094513 (2015), arXiv:1507.02162 [cond-mat.dis-nn].
- [54] G. Cossu and S. Hashimoto, *JHEP* **06**, 056 (2016), arXiv:1604.00768 [hep-lat].
- [55] M. Giordano, T. G. Kovacs, and F. Pittler, (2026), arXiv:2602.10921 [hep-lat].
- [56] J. T. Edwards and D. J. Thouless, *Journal of Physics C: Solid State Physics* **5**, 807 (1972).
- [57] R. V. Gavai, M. E. Jaensch, O. Kaczmarek, F. Karsch, M. Sarkar, R. Shanker, S. Sharma, S. Sharma, and T. Ueding, *Phys. Rev. D* **111**, 034507 (2025), arXiv:2411.10217 [hep-lat].
- [58] A. Bazavov, N. Brambilla, H. T. Ding, P. Petreczky, H. P. Schadler, A. Vairo, and J. H. Weber, *Phys. Rev. D* **93**, 114502 (2016), arXiv:1603.06637 [hep-lat].
- [59] V. Oganesyan and D. A. Huse, *Phys. Rev. B* **75**, 155111 (2007).
- [60] O. Giraud, N. Macé, E. Vernier, and F. Alet, *Phys. Rev. X* **12**, 011006 (2022).
- [61] R. G. Edwards, U. M. Heller, J. E. Kiskis, and R. Narayanan, *Phys. Rev. D* **61**, 074504 (2000), arXiv:hep-lat/9910041.
- [62] E. Hofstetter and M. Schreiber, *Phys. Rev. B* **48**, 16979 (1993).
- [63] F. J. Dyson, *J. Math. Phys.* **3**, 1191 (1962).
- [64] C. M. Canali, *Phys. Rev. B* **53**, 3713 (1996).
- [65] V. Kravtsov and K. Muttalib, *Physical review letters* **79**, 1913 (1997).
- [66] H. Yan, *Phys. Rev. E* **111**, 054213 (2025).
- [67] N. Rosenzweig and C. E. Porter, *Phys. Rev.* **120**, 1698 (1960).
- [68] T. A. Brody, J. Flores, J. B. French, P. A. Mello, A. Pandey, and S. S. M. Wong, *Rev. Mod. Phys.* **53**, 385 (1981).
- [69] G. Lenz and F. Haake, *Phys. Rev. Lett.* **67**, 1 (1991).
- [70] V. K. B. Kota and S. Sumedha, *Phys. Rev. E* **60**, 3405 (1999).
- [71] S. Schierenberg, F. Bruckmann, and T. Wettig, *Phys. Rev. E* **85**, 061130 (2012), arXiv:1202.3925 [math-ph].
- [72] F. Bruckmann, T. G. Kovacs, and S. Schierenberg, *Phys. Rev. D* **84**, 034505 (2011), arXiv:1105.5336 [hep-lat].
- [73] M. Giordano, T. G. Kovacs, and F. Pittler, *JHEP* **04**, 112 (2015), arXiv:1502.02532 [hep-lat].

- [74] R. N. Larsen, S. Sharma, and E. Shuryak, *Phys. Rev. D* **105**, L071501 (2022), arXiv:2112.04537 [hep-lat].
- [75] R. N. Larsen, S. Sharma, and E. Shuryak, *Phys. Lett. B* **794**, 14 (2019), arXiv:1811.07914 [hep-lat].
- [76] R. N. Larsen, S. Sharma, and E. Shuryak, *Phys. Rev. D* **102**, 034501 (2020), arXiv:1912.09141 [hep-lat].
- [77] J.-P. Blaizot and M. A. Nowak, *Phys. Rev. Lett.* **101**, 102001 (2008), arXiv:0801.1859 [hep-th].
- [78] S. Guin, H. Pandey, and S. Sharma, *Phys. Lett. B* **866**, 139490 (2025), arXiv:2501.04397 [hep-lat].
- [79] D. Basko, I. Aleiner, and B. Altshuler, *Annals of Physics* **321**, 1126 (2006).
- [80] D. A. Abanin, E. Altman, I. Bloch, and M. Serbyn, *Rev. Mod. Phys.* **91**, 021001 (2019).
- [81] S. Bera, H. Schomerus, F. Heidrich-Meisner, and J. H. Bardarson, *Phys. Rev. Lett.* **115**, 046603 (2015).
- [82] A. Smith, J. Knolle, D. L. Kovrizhin, and R. Moessner, *Phys. Rev. Lett.* **118**, 266601 (2017).
- [83] J. H. Pixley, P. Goswami, and S. Das Sarma, *Phys. Rev. Lett.* **115**, 076601 (2015).
- [84] F. von Oppen, *Phys. Rev. Lett.* **73**, 798 (1994).
- [85] M. A. Clark, R. Babich, K. Barros, R. C. Brower, and C. Rebbi (QUDA), *Comput. Phys. Commun.* **181**, 1517 (2010), arXiv:0911.3191 [hep-lat].
- [86] C. Lehner, M. Bruno, D. Richtmann, M. Schlemmer, R. Lehner, D. Knüttel, T. Wurm, L. Jin, S. Bürger, A. Hackl, and A. Klein, “Grid Python Toolkit (GPT), 2024-10,” (2024).